Superalloys 2012: 12th International Symposium on Superalloys
Edited by: Eric S. Huron, Roger C. Reed, Mark C. Hardy, Michael J. Mills, Rick E. Montero, Pedro D. Portella, Jack Telesman
TMS (The Minerals, Metals & Materials Society), 2012

Interfaces in Ni-base superalloys and implications for mechanical behavior and environmental embrittlement: a first-principles study

Suchismita Sanyal[1], Umesh V. Waghmare[2], Timothy Hanlon[3], Ernest L Hall[3], PR Subramanian[3] and Michael F.X. Gigliotti[3]

[1]GE Global Research, Hoodi Village, Whitefield Road, Bangalore 560066, India
[2]Theoretical Sciences Unit, Jawaharlal Nehru Centre for Advanced Scientific Research, Jakkur, Bangalore 560 064, India
[3]GE Global Research, 1 Research Circle, Niskayuna NY12309, USA

Keywords: First-principles; nickel based superalloys; interfaces; grain boundaries; Oxygen; Embrittlement;

Abstract

Motivated by the vital role played by grain boundaries and interfaces in Ni-based superalloys in influencing mechanical properties such as creep rupture strength, fatigue crack growth rates and resistance towards environmental embrittlement, we use first-principles simulations to estimate fracture strengths of Ni Σ3(111) grain boundary, Ni Σ5(012) grain boundary, Ni/Ni_3Al interfaces and Ni/boride interfaces through determination of their work of separation. We find that Ni/boride interfaces have higher fracture strengths than the other commonly occurring interfaces in Ni-alloys, such as NiΣ5 & NiΣ3 grain boundaries and coherent Ni/Ni_3Al interfaces, and are less susceptible to oxygen-induced embrittlement. Our calculations show how the presence of Mo at Ni/M_5B_3 (M = Cr, Mo) interfaces leads to additional reduction in oxygen-induced embrittlement. Through Electron-Localization-Function based analyses, we identify the electronic origins of effects of alloying elements on fracture strengths of these interfaces and observe that chemical interactions stemming from electronegativity differences between different atomic species are responsible for the trends in calculated strengths. Our findings should be useful towards designing Ni-based alloys with higher interfacial strengths and reduced oxygen-induced embrittlement.

Introduction

In multi-element Ni-base superalloys used in high-temperature applications such as turbine disks, microstructures consist of multiple phases, such as γ', γ'', carbides, borides [1]. Complex interfaces, including γ/γ grain boundaries, γ/γ' interfaces and γ/Boride interfaces coexist in Ni-based superalloys in different proportions, depending on alloying, processing and heat-treatment conditions. These interfaces and grain boundaries have been found to play a critical role in controlling the bulk mechanical properties of these alloys [2]. Hence, to gain a more complete understanding of the mechanical responses of these alloys in terms of resistance to crack propagation through interfaces/grain boundaries, it is insightful to compare the fracture strengths of the various interfaces/grain boundaries.

Under certain combinations of stress and temperature, many materials will tend to fail in an intergranular fashion [3]. A proposed solution to this problem has been to percolate the microstructure with boundaries having an increased resistance to fracture, via appropriate processing routes [4]. A simplified way to characterize a grain boundary between two grains involves the coincidence-site-lattice (CSL) model, in which the relative orientation of the two grains is given by a ΣN value, where one out of N atoms along the grain boundary is coincident [5]. Hanada *et al* [6] and Lin *et al* [7] have established that in Ni_3Al, low-angle and Σ3 symmetrical boundaries are especially resistant to cracking and therefore are considered as "strong boundaries". J. Q. Su *et al* [8] furthered this study by establishing that while Σ1, Σ3, and Σ9 boundaries in Ni3Al are crack-resistant, Σ5, Σ7, Σ11, Σ13 and random boundaries are weaker, fracturing preferentially to the bulk intragranular material. These studies qualitatively establish a relationship between fracture properties and the type of grain boundary based on its Σ-value. However, to the best of our knowledge, there has been no modeling study around prediction of fracture strengths and their correlation with grain boundary character distribution.

The susceptibility of Ni-based superalloys as well as Ni-Ni_3Al based alloys to environmental embrittlement is well documented [9-10]. Ni-based superalloys can experience accelerated crack growth rates under the combined effects of environment, stress, and temperature [1, 11-14]. Careful experiments done on air-exposed Ni270 (99.98 pct Ni) specimens exhibit large regions of intergranular failure, contrasted with their vacuum-exposed counterparts which show ductile behavior [14].

Addition of boron is reported to be beneficial in reducing environmental embrittlement in various Ni-based superalloys [15-16]. B atoms are found to segregate to grain boundaries and bind to grain boundary sites, or precipitate as boride particles along grain boundaries in Ni-base superalloys [17]. Considering the potential impact of borides at grain boundaries on mechanical responses of Ni-based alloys [17-19], an understanding of the fracture strengths of boride-containing interfaces has become critical.

Experimentally, a sample always contains different types of grain boundaries and interfaces and it is hard to study their relative strengths and role in determining fracture behavior or embrittlement. Over the last decade, there has been a significant amount of theoretical work developing relationships between specific Ni-based superalloy interfaces and their bulk mechanical properties. For example, sulfur-induced embrittlement of Ni has been studied by Yamaguchi *et al* [20] through first-principles calculation of grain boundary decohesion in Ni-Σ5(012). However, the fracture strength of Ni grain boundaries as a function of environmental effects and grain boundary character distribution has not been studied in details. The next predominant interface in Ni-base superalloys is the γ/γ' interface as a typical microstructure contains ~50% of its volume fraction as γ' precipitates. The γ/γ'interface has been widely studied using first-principles quantum mechanical calculations to investigate the strengthening mechanisms of a variety of alloying metal

substitutions [21-24], while similar studies of γ/boride interfaces have not been reported as yet.

The aim of this work is to establish a procedure of providing a comparative study of cohesive strengths of γ/γ grain boundaries, γ/γ' interfaces and γ/boride interfaces and examine the effects of environmental embrittlement on select interfaces using first-principles density functional calculations. Σ3(111) symmetrical tilt boundaries and Σ5(012) grain boundaries are chosen to evaluate effects of grain boundary character on the fracture strengths of γ/γ grain boundaries. This paper builds on our previous work on Ni-Σ5(012) grain boundaries [25], Ni/Ni_3Al interfaces [26] and Ni/boride interfaces [27] and incorporates the effects of Ni-Σ3(111) grain boundaries towards comprehensive comparative insights.

This paper is organized as follows. The methodology including a description of the first-principles based computational technique and details of creation of the grain boundaries/interfaces and is described in Section 2. Discussions are provided in Section 3. Our findings are summarized in Section 4.

Methodology

Computational Details

We use first-principles Density Functional Theory [28-29], as implemented in the Vienna Ab initio Simulation Package (VASP) [30], with the Perdew-Wang [31] function of the Generalized Gradient Approximation (GGA) to exchange-correlation energy, with no dependence on electronic spin. Projector-augmented wave potentials [32] are used to describe the computationally expensive electron-ion interactions, which permitted the use of a plane-wave basis set with energy cutoff of 400 eV in the representation of the Kohn-Sham wave functions. The Brillouin Zone integrations are sampled with a 3x3x2 Monkhorst-Pack grid [33] in a calculation with supercell consisting of 80 atoms; this amounts to use of a Born von Karman periodic cell with 720 atoms or use of a 9x9x9 mesh of k-points in integration over Brillouin Zone of a calculation with cell containing one atom. Ground-state atomic geometries for all structures are obtained by minimizing the energy until the magnitude of Hellman-Feynman forces [34] are less than a tolerance of 0.01 eV/Å per atom. To ensure the precision of energies and geometries, k-point and plane-wave cutoff energy convergence tests are performed, showing convergence of total energies within 1-2 meV per atom.

Structures

In the structural models, the γ-phase is assumed to consist of FCC Ni, with theoretical lattice constant a_{Ni} = 3.51 Å.

The Σ3(111) symmetric Ni grain boundary is created by first cleaving FCC Ni along the (111) plane. One half of the separated crystal was then reflected in the surface plane. The two grains were then joined after the removal of overlapping atoms to produce the desired Σ3(111) structure consisting of 72 atoms (Fig. 1(a)). Following a similar procedure, the Σ5(012) Ni grain boundary is constructed, consisting of 80 atoms (Fig. 1(b)).

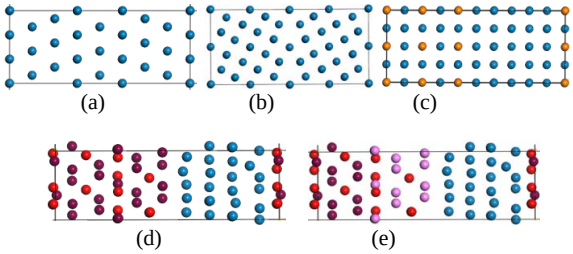

Figure 1. (Color Online)Structural configurations of grain boundaries and interfaces studied (a) Ni Σ3(111) grain boundary (b) Ni Σ5(012) grain boundary (c) coherent Ni/Ni_3Al interface, (d) Ni/Cr_5B_3 interface and (e) Ni/$(CrMo)_5B_3$ interface. Ni, Al, Cr, Mo and B atoms are denoted by blue, orange, brown, pink and red color.

Structural optimization of L_{12} Ni_3Al yielded lattice constant a_{Ni3Al} = 3.57 Å, which is in excellent agreement with the experimental values [35]. In the interfacial plane, 2x2 supercells of each of Ni and Ni_3Al are used to create a perfectly lattice coherent Ni/Ni_3Al interface with a lattice constant of 3.54 Å. A periodic supercell with two Ni/Ni_3Al interfaces, consisting of 80 atoms, is used in the calculations (Fig. 1c).

Finally, the γ/Boride interface is created based on reported experimental data on the orientation relationships of boride precipitates with γ-grain boundaries. Zhang *et al* [36-37] have carried out extensive characterization of IN738 and Rene 80 to establish the boride precipitates along γ-grain boundaries to be Cr_5B_3-type M_5B_3, with a BCT structure and lattice parameters of a = 5.4 Å, c = 10.1 Å, and c/a = 1.83. They have carried out compositional analysis by x-ray spectroscopy in the transmission electron microscope to establish that the primary constituents of these borides are Cr, Mo & W. Structural optimization of bulk relaxations of I4/mcm Cr_5B_3 yielded lattice constants a_{Cr5B3} = 5.37 Å and c_{Cr5B3} = 10.18 Å which are in excellent agreement with the experimental values of a_{Cr5B3} = 5.4 Å, c_{Cr5B3} = 10.1 Å, respectively. Based on these bulk configurations and the orientation relationship of the γ/Boride interface being variants of $(001)_\gamma$ ll $(001)_{M5B3}$, the Ni/Cr_5B_3 interface has been constructed, consisting of 8 atomic planes of Cr_5B_3 and 4 atomic planes of FCC Ni, i.e. 52 atoms (Fig. 1(d)). This semi-coherent interface has a lattice constant of a = 5.46 Å with a lattice mismatch of Δa = 1.1% with Cr_5B_3. The effect of boride chemistry on interfacial strength is studied through a 50% Mo-for-Cr substitution within the Cr_5B_3 boride (Fig. 1(e)), see ref. [27] for details.

The fracture strength of an interface between grains X and Y is assessed through determination of the cleavage energy, γ_{cl}^{XY}. γ_{cl}^{XY} is essentially the *work of separation* [38] and defined as

$$\gamma_{cl}^{XY} = \gamma_s^X + \gamma_s^Y - \frac{E_{int}}{2A}$$

For example, for an interface between Ni and Boride, cleavage energy is given by $\gamma_{cl}^{Ni/Boride}$ where,

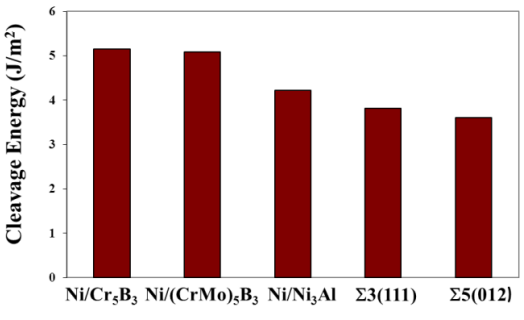

Figure 2. Calculated Cleavage Energies for Σ5(012) Ni grain boundary, Σ3(111) Ni grain boundary, Ni/Ni_3Al interface and Ni/M_5B_3 (M = Cr, Mo) interfaces.

$$\gamma_{cl}^{Ni/Boride} = \gamma_s^{Ni} + \gamma_s^{Boride} - \frac{E_{int}}{2A}$$

where, E_{int} is the energy of the supercell with model γ/M_5B_3 (M=Cr, Mo) interface with respect to their bulk energies with same number of atoms, A is the area of the supercell, γ_s^{Ni} and γ_s^{Boride} are the surface energies of Ni and Boride respectively. For a grain boundary, X and Y correspond to different crystallographic orientations of the same material. The details of cleavage planes and process of cleaving of these grain boundaries and interfaces are published elsewhere [25-27].

Results and Discussion

Comparison of fracture strengths of grain boundaries and interfaces

Calculated cleavage energies for the pure grain boundaries and interfaces are given in Figure 2. A comparison between the two grain boundaries examined in Ni points to the direction that Ni Σ 3(111) symmetric tilt boundaries need higher energies to cleave the boundary over Ni Σ5(012), thereby indicating that Σ3(111) symmetric tilt boundaries are stronger than Σ5(012) in pure Ni. This finding is in accordance with experimental observations. Suzuki *et al* [39] experimentally determined the fracture strengths of different CSL grain boundaries in Ni-20Cr using a microtensile test method to show the fracture strength of Σ3(111) grain boundaries are higher than that of Σ5(012) boundaries. Our finding is also consistent with experimental measurements of grain boundary fracture strengths done on FCC intermetallic compound Ni_3Al where Su *et al* [8] report the fracture strengths of Σ3 grain boundaries to be higher than that of Σ5.

A comparison of cleavage energies across Ni/Cr_5B_3 interfaces, Ni/Ni_3Al interfaces, Ni-Σ5(012) grain boundaries and Ni-Σ3(111) grain boundaries reveals notable trends.. The cleavage energy of Ni/Cr_5B_3 and Ni/$Cr_{2.5}Mo_{2.5}B_3$ interfaces (5.15 & 5.08 J/m^2, respectively) is found to be higher than those obtained for the Ni/Ni_3Al interface (4.22 J/m^2) and Ni grain boundaries (3.60 & 3.81 J/m^2). This indicates that fracture strengths of the Ni/Boride

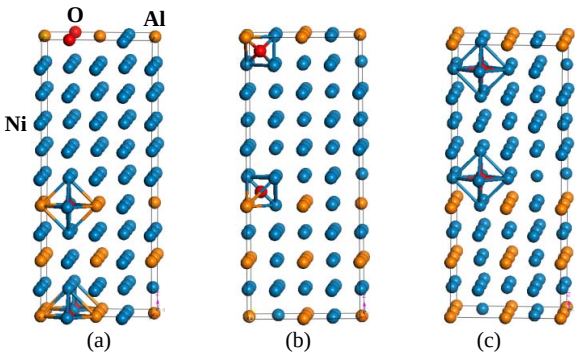

Figure 3. (Color Online) Ni/Ni_3Al interface with O at various available interstitial sites: (a) Ni-Al octahedral site (b) Ni-Al tetrahedral site and (c) all-Ni octahedral site at the interface. Ni, Al, and O atoms are denoted by blue, orange, and red, respectively [Ref. 26]

interfaces are intrinsically higher than that of NiΣ5 & Σ3 grain boundaries and coherent Ni/Ni_3Al interfaces in Ni-base alloys. This finding is consistent with experimental observations that addition of B increases the creep rupture strength and decreases the fatigue-crack-growth rates in Ni-base superalloys [15, 18]. Rosler *et al* [15] demonstrated significant life extension in INCONEL 706 by chemical modification of a surface zone with B and established that the B was present as boride precipitates in the matrix zone. Xiao *et al* [18] reported that addition of B improved the crack growth resistance of IN 718 at room temperature and at 650^0C. With increasing B concentration, the fracture mode in these alloys was found to change from intergranular- to transgranular, indicating a change in interfacial cohesion.

It is interesting to compare our current findings with earlier calculations, where we had placed B as an interstitial dopant along a Ni-Σ5(012) grain boundary, at a concentration of 2.4 atomic% [30]. The cleavage energy of Ni-Σ5(012) grain boundary with atomic B (3.82 J/m^2) was found to be higher than that of a undoped grain boundary (3.60 J/m^2), thereby establishing that even during equilibrium segregation of B at grain boundaries, B acts as a strengthener. During non-equlibrium segregation when B is present as boride precipitates along grain boundaries [17], the strengthening effect is found to be even higher, as is evident in the cleavage energy of Ni/Cr_5B_3 interfaces (5.15 J/m^2, Figure 2).

Effects of oxygen embrittlement

To study the effects of oxygen on interfacial strength, Ni/Ni_3Al and Ni/M_5B_3 (M = Cr, Mo) interfaces are chosen.

In the Ni/Ni_3Al interface, oxygen segregation is studied by placing one oxygen atom at each of the interfaces, resulting in an impurity concentration of 2.5 atomic%. There are three possible interstitial sites for occupancy by the impurity atoms at the interface, viz. a tetrahedral site constituted by 3 Ni and 1 Al atom; an octahedral site formed by 6 Ni atoms, and another octahedral site formed by 4 Ni and 2 Al atoms (see Figure 3). The interstitial volumes decrease in the order:

6Ni Octahederal site > 4Ni-2Al Octahedral site > 3Ni-1Al tetrahedral site.

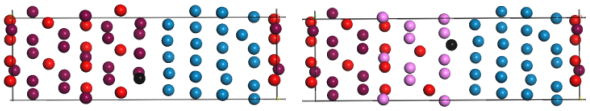

(a) (b)

Figure 4. (Color Online) Configurations of (a) Cr_5B_3/Ni interface and (b) $(Cr,Mo)_5B_3$/Ni with O atom along the interfaces. Ni, Cr, B, Mo and O atoms are denoted by blue, red, brown, pink and black color. Ref. [27]

Despite the above, the most favorable site for O residence is found to be the 4 Ni-2Al octahedral site, followed by the 3Ni-1Al tetrahedral site and the all-Ni octahedral site. Hence the preferred sites at the interstices of Ni/Ni_3Al interface for an O dopant seem to be guided more by the chemical interactions than the interstitial space availability. This can be explained by the strong chemical affinity of electronegative O towards Al atoms, which is found to govern its preferences for its nearest neighbors, dictating its interstitial site preferences. The tendency of O to segregate to the γ/γ' interface over residing in the bulk lattice can be determined from the energy difference ΔE, given by:

$$\Delta E = E^{int}(Ni_{68}Al_{12}O_2) - [\, E^{bulk}(Ni_{32}O) + E^{bulk}(Ni_{36}Al_{12}O)],$$

where, $E^{int}(Ni_{68}Al_{12}O_2)$ is the total energy of γ/γ' interface having oxygen at its preferred interstitial site, $E^{bulk}(Ni_{32}O)$ is the total energy of oxygen in the preferred interstitial site of bulk FCC Ni, $E^{bulk}(Ni_{36}Al_{12}O)$ is the total energy of oxygen in the preferred interstitial site of bulk L_{12} Ni_3Al. Our calculations show that O has a strong natural tendency to segregate to the γ/γ' interface (-0.41 eV).

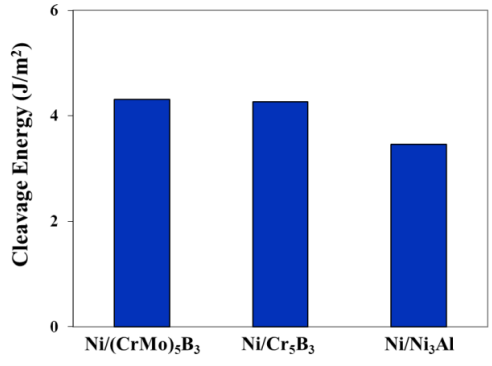

Figure 5. Calculated Cleavage Energies for Ni/Ni_3Al and Ni/Cr_5B_3 (M = Cr, Mo) interfaces, with oxygen.

Cleavage energies for the Ni/Ni_3Al & Ni/M_5B_3 (M = Cr, Mo) interfaces with oxygen at the different preferred sites at the interface are given in Figure 5. A comparison with cleavage energies calculated for undoped Ni/Ni_3Al & Ni/M_5B_3 (M = Cr, Mo) interfaces (Figure 2) show that with introduction of oxygen, there is reduction in cleavage energies in all interfaces, indicating that both Ni/Ni_3Al & Ni/M_5B_3 (M = Cr, Mo) interfaces are weakened. However, the cleavage energy of Ni/Ni_3Al interfaces in the presence of oxygen (3.46 J/m^2) is lower than that of Ni/boride interfaces in the presence of oxygen (4.27-4.31 J/m^2, Figure 5). This suggests that the extent of environmental embrittlement in γ/boride interfaces is lesser than in γ/γ' interfaces. This result is broadly supported by earlier experimental work on IN706 where O-enhanced-crack-growth rate is lowered by increasing surface concentration of B, which is found to form boride precipitates within the matrix [15].

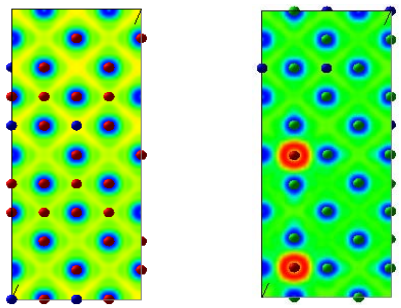

(a) (b)

Figure 6. Electron Localization Function distributions for (a) pure Ni/Ni_3Al interface and (b) with oxygen at the interface. Ref. [26]

To assess whether O would spontaneously like to go to a Ni/Ni_3Al interface over a Ni/Boride interface, the following energies are estimated:

$$E(Ni/Ni_3Al\text{-}O) = E(Ni/Ni_3Al + O) - E(Ni/Ni_3Al) - E(O) \quad (i)$$

$$E(Ni/Cr_5B_3\text{-}O) = E(Ni/Cr_5B_3 + O) - E(Ni/Cr_5B_3) - E(O) \quad (ii)$$

$$E(Ni/Cr_{2.5}Mo_{2.5}B_3\text{-}O) = E(Ni/Cr_{2.5}Mo_{2.5}B_3 + O) -$$

$$E(Ni/Cr_{2.5}Mo_{2.5}B_3) - E(O) \quad (iii)$$

Our estimates for these energies are calculated to be -10.58 eV, -6.63 eV and -5.66 eV for (i), (ii) and (iii) respectively. These estimates demonstrate that an O atom prefers to be at the Ni/Ni_3Al interface over Ni/Cr_5B_3 interface by 3.94 eV. Comparison of (i) & (iii) also establishes that O prefers to be at the Ni/Ni_3Al interface over $Ni/Cr_{2.5}Mo_{2.5}B_3$ interface by 4.92 eV. This finding, along with our earlier observation that the effect of O-induced embrittlement is much more severe in Ni/Ni_3Al interfaces than in Ni/Cr_5B_3 interfaces indicates a potential pathway for improving intergranular crack growth resistance in Ni-base superalloys by way of increasing the volume fraction of grain boundary borides.

<u>Effect of composition of boride on γ/Boride interfacial fracture strengths</u>

Based on these calculations, an understanding of the effects of chemistry on the fracture strengths of Ni/Ni_3Al & Ni/M_5B_3 (M = Cr, Mo) interfaces is developed through an examination of the electron localization functions [40] (ELF) (see Figs. 6 & 7). The relative interplay of electronegativities (EN) between the different

atomic species (Ni, Cr, Mo, B, O) is found to hold a key to their interfacial strengths. For pristine Ni/Cr_5B_3 interfaces in the absence of O, charge transfer across the interface, and hybridization between dissimilar atoms, leads to higher fracture strength than that calculated for a Σ5(012) Ni grain boundary, Σ3(111) Ni grain boundary or a Ni/Ni_3Al interface (see Figure 2). Addition of Mo to the boride reduces the Ni/boride interface strength in the absence of O because of a reduced EN difference between B and Ni. This is a direct consequence of a higher electronegativity of Mo, relative to Cr (EN of Cr = 1.66, EN of Mo = 2.16, EN of Ni = 1.91, EN of B = 2.04, in Pauling Scale).

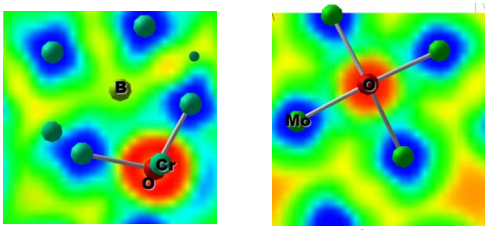

(a) (b)

Figure 7. (Color Online) Contour plots of Electron Localization Function in (001) plane for (a) Cr_5B_3/Ni interface and (b) $(Cr,Mo)_5B_3$/Ni interface with oxygen. Extent of charge localization induced by oxygen in the two cases may attribute to the differential strengths of these interfaces. Ref. [27]

O is found to induce a strong region of charge concentration around itself when present at an interface (Figs. 6 & 7). It had earlier been established [29-31] that charge localization around a dopant at the interface results in increased ionicity at the interface, thus weakening the interface. A similar region of charge concentration is seen around O in the Ni/Cr_5B_3 interface (Figure 7) attributing to its embrittlement.

Oxygen, a strongly electronegative element (EN of O = 3.44, in Pauling Scale) in the Ni/Cr_5B_3 interface is predicted to pull electrons from Cr leading to charge localization around O atoms. In contrast, in the Ni/$Cr_{2.5}Mo_{2.5}B_3$ interface, the presence of electronegative Mo suppresses the strong electronegative character of O to some extent, resulting in less charge localization around O, which is reflected in the increased strength of the Ni/$Cr_{2.5}Mo_{2.5}B_3$ interface, relative to its Ni/Cr_5B_3 counterpart, in the presence of O. The extent of charge localization around O atoms in these two interfaces is evident in the ELF plots (see Fig. 7). It is also interesting to note that although the starting positions of O atoms are kept identical in Ni/Cr_5B_3 and Ni/$Cr_{2.5}Mo_{2.5}B_3$ interfaces, upon relaxation O atoms approach Cr atoms, the most electropositive atom in the Ni/Cr_5B_3 interface. However, for the Ni/$Cr_{2.5}Mo_{2.5}B_3$ case, where the interface is comprised of Ni, Mo & B atoms with Cr atoms positioned farther from the interface, O is found to move further from Mo, positioning itself at an intermediate position between Ni & B atoms. This shift in priority demonstrated by the O atom is directly related to the relative electronegativities of its nearest neighbor atoms. This synergistic interplay between different alloying elements present in the interfaces is found to ultimately influence the strength of these interfaces.

Conclusions

In summary, first-principles calculations are used to determine the fracture strengths of γ/γ' interfaces, γ/γ grain boundaries and γ /boride interfaces in Ni-based superalloys. We show that (a) fracture strengths of Ni/boride interfaces are higher than the Ni-Σ5 grain boundaries and coherent Ni/Ni_3Al interfaces in Ni-based alloys, (b) Ni/boride interfaces are more resistant towards O-embrittlement than coherent Ni/Ni_3Al and (c) (Cr,Mo)Borides are more effective in reducing O-induced embrittlement in Ni/M_5B_3 interfaces, than their Cr-Boride counterparts. The cause and relative extents of embrittlement of Ni/M_5B_3 (M = Cr, Mo) interfaces are found to correlate well with the levels of ionic charge concentration around O, and can be understood in terms of electronegativities of different atomic species at the interface.

Future work in this area would involve exploring different orientation relationships in γ/boride interfaces and also incorporating other variants such as γ/boride interfaces, to develop a more complete understanding of the effects of boride precipitates in the microstructures of Ni-based superalloys. Keeping in mind the synergistic interplay between different alloying elements and their effects on mechanical responses of interfaces, it would be interesting to extend the current calculations beyond Ni to capture the effect of multi-element γ composition on interfacial strengths.

Our work provides a framework for fundamental understanding of fracture strengths of relevant interfaces in Ni-based superalloys, and should help in identifying alloying additions/processing routes to increase the strengths and proportions of such interfaces. Such approaches would work towards increasing the overall strength of Ni-based superalloys and reducing their environmental sensitivity during service.

Acknowledgement

This work is supported by the Nanotechnology Advanced Technology program of GE Global Research. The authors thank M. Blohm for useful discussions during the course of this work. UW thanks GE Global Research for an unrestricted research grant.

References

1. R.C. Reed, The Superalloys – Fundamentals and Applications, first ed., Cambridge University Press, Cambridge, UK, 2006.
2. E. S. Huron, K. R. Bain, D. P. Mourer, J. J. Schirra, P. L. Reynolds and E. E. Montero, "Superalloys 2004", ed. K.A. Green *et al* (The Minerals, Metals and Materials, 2004), 73.
3. C. T. Liu, C. L. White and J.A. Horton, Acta. Metall. 33 (1985) 213.
4. T. Watanabe, Mater. Forum 11 (1988) 284.
5. S. Ranganathan, Acta Cryst. 21 (1966) 197.
6. S. Hanada, S. Watanabe and O. Izumi, J. Mater. Sci. 21 (1986) 203.
7. H. Lin and D. P. Pope, Acta. Metall. Mater. 41 (1993) 553.
8. J. Q. Su, M. Demura and T. Hirano, Mate. Res. Soc. Symp. Proc. 646 (2001) N6.10.1.
9. C. T. Liu, Scripta Metall Mater 27 (1992) 25.
10. D. A. Woodford, Energy Mater. 1 (2006) 59.

11. R. P. Wei, C. Miller, Z. Huang, G. W. Simmons, D. G. Harlow, Engg Fract Mech 76 (2009) 695.
12. R. Molins, J.-C. Chassaigne and E. Andrieu, in “Superalloys 718, 625, 706 and various derivatives”, E.A. Loria (eds.), TMS (1997) 655.
13. E. Andrieu, G. Hochstetter, R. Molins and A. Pineau in “Superalloys 718, 625, 706 and various derivatives”, E.A. Loria (eds.), TMS (1994) 619.
14. D.A. Woodford and R.H. Bricknell, Met. Trans. 12A (1981) 1467.
15. S. Muller and J. Rosler: in ‘Life assessment of hot section gas turbine components’, (ed. R. Townsend *et al*), IOM Communications, London, 1999, pp 49-60.
16. T.J. Garosshen, T.D. Tillman, G.P. McCarthy, Metall. Trans. 18A (1987) 69.
17. W. Chen, M.C. Chaturvedi, N.L. Richards, G. McMahon, Metall Trans A 29 (1998) 1947.
18. L. Xiao, D.L. Chen and M.C. Chaturvedi, Mater. Sci. Engg A 428 (2006) 1.
19. L. Xiao, D.L. Chen and M.C. Chaturvedi, Superalloys 2004, Edited by K.A. Green, T.M. Pollock, H. Harada, TMS (2004) 275.
20. M. Yamaguchi, M. Shiga and H. Kaburaki, Science 307 (2005) 393.
21. K. Chen, L. R. Zhao, J. S. Te, Mater Sci. Engg. A 365 (2004) 80.
22. P. Peng, D.W. Zhou, J.S. Liu, R. Yang, Z.Q. Hu, Mater Sci. Engg. A 416 (2006) 169.
23. Yun-Jiang Wang, Chong-Yu Wang, Mater Sci. Engg. A 490 (2008) 242.
24. Y. Liu, K. Y. Chen, G. Lu, J. H. Zhang, Z. Q. Hu, Acta Mater 45 (1997) 1837.
25. S. Sanyal, U. V. Waghmare, P. R. Subramanian, M. F. X. Gigliotti, Appl. Phys. Lett. 93 (2008) 223113.
26. S. Sanyal, U. V. Waghmare, P. R. Subramanian, M. F. X. Gigliotti, Scripta Mater. 63 (2010) 391.
27. S. Sanyal, U. V. Waghmare, T. Hanlon, E.L.Hall, Mat. Sci. Engg. A. 530 (2011) 373.
28. P. Hohenberg, W. Kohn, Phys Rev B136 (1964) 864.
29. W. Kohn, L. J. Sham, Phys Rev 140 (1965) A1133.
30. G. Kresse, J. Furthmüller, Phys Rev B54 (1996) 11 169.
31. J. P. Perdew, J. A. Chevary, S. H. Vosko, K. A. Jackson, M. R. Pederson, D. J. Singh, C. Fiolhais, Phys Rev B46 (1992) 6671.
32. P.E. Blöchl, Phys Rev B50 (1994) 17953.
33. H. J. Monkhorst, J. D. Pack, Phys Rev B13 (1976) 5188.
34. R. P. Feynman, Phys Rev 56 (1939) 340.
35. A. Taylor, R.W. Floyd, J. Inst. Met. 81 (1952) 25.
36. H.R. Zhang, O.A. Ojo, J Mater Sci 43 (2008) 6024.
37. H.R. Zhang, O.A. Ojo, M.C. Chaturvedi, Scripta Mater. 58 (2008) 167.
38. J. P. Hirth, Phil. Trans. R. Soc. Lond. A 295 (1980) 139.
39. A. Suzuki, M. F. X. Gigliotti, P. R. Subramanian, Scripta Mater. 64 (2011) 1063.
40. Savin, J. Mol. Str: Theochem 727 (2005) 127.